Appl. Phys. B 82, 419–422 (2006)
DOI: 10.1007/s00340-005-2002-3

Applied Physics B
Lasers and Optics

K. PEITHMANN[1,✉]
M.-R. ZAMANI-MEYMIAN[1]
M. HAAKS[1]
K. MAIER[1]
B. ANDREAS[2]
K. BUSE[2]
H. MODROW[3]

Fabrication of embedded waveguides in lithium-niobate crystals by radiation damage

[1] Helmholtz-Institut für Strahlen- und Kernphysik, Universität Bonn, Nussallee 14–16, 53115 Bonn, Germany
[2] Physikalisches Institut, Universität Bonn, Wegelerstr. 8, 53115 Bonn, Germany
[3] Physikalisches Institut, Universität Bonn, Nussallee 12, 53115 Bonn, Germany

Received: 11 August 2005
Published online: 6 December 2005 •

ABSTRACT Irradiation of lithium-niobate crystals ($LiNbO_3$) with fast, high-energy ^{3}He ions changes the refractive index in the interaction region where the ions speed through the material. Thus an inhomogeneous flux density profile can be used for a tailored modification of the optical properties of $LiNbO_3$ crystals, without employing ion implantation. A new method to fabricate embedded, polarization sensitive channel waveguides in $LiNbO_3$ utilizing accelerated ^{3}He ions with an energy of 40 MeV is demonstrated.

PACS 78.20; 42.82

1 Introduction

Lithium-niobate crystals ($LiNbO_3$) play an important role as a source material for optical devices due to their mechanical robustness, good availability, optical homogeneity, and advantageous ferroelectric, electro-optic, and photorefractive properties. Applications like holographic filters [1–3] and holographic storage devices [4, 5] have drawn a lot of attention. Integrated optics with lasers, modulators, and filters on a single $LiNbO_3$ wafer [6–10] are especially promising. To integrate optical components on $LiNbO_3$, powerful techniques for the fabrication of waveguides are needed to be able to guide, control, and modify the light. Standard techniques that provide high-quality waveguides are proton exchange [11] and indiffusion of titanium [12, 13]. These treatments enhance the refractive index next to the surface of the crystals and thus enable the guiding of light in a thin layer (thickness in the order of 10 μm) between the surface and the bulk material. Implantation of low-energy ions (with energies ≈ 2 MeV) is another technique to create waveguiding structures [14] with the waveguiding layer being formed between the crystal surface and the stop layer of the implanted ions, where the refractive index is strongly diminished due to large energy loss of the ions in a small volume. All techniques described so far yield waveguides using the crystal surface as one refractive index step; thus, the waveguides are placed directly below the surface.

✉ Fax: +49 228 73 2505, E-mail: peithmann@hiskp.uni-bonn.de

We present a different approach: Treating $LiNbO_3$ with high-energy particles (about 40 MeV) changes the refractive index n in the regions in front of the Bragg peak where the ions transmit through the material [15]. Hence the refractive index is changed in all layers right from the surface down to the stop depth, which is caused by radiation damage. Strong changes in the order of $\Delta n \approx 3 \times 10^{-3}$ are possible, and the changes are reasonably stable at room temperature whereas they can be erased by annealing the crystals at 500 °C. The implantation range for these high energy ions in $LiNbO_3$ is about 0.6 mm. Using spatially inhomogeneous flux densities yields spatially modulated refractive-index profiles which allow one to tailor planar and channel waveguides that are embedded within the material. Real three-dimensional structures can be manufactured as a consequence of the high particle momentum and the low angular scattering.

2 Experimental methods

We use $LiNbO_3$ crystals that are prepared from commercially available, undoped wafer material (thickness 1 mm). Pieces of $5 \times 6\,\mathrm{mm}^2$ are cut, where the 6 mm side is oriented parallel to the crystallographic c axis. The surfaces are polished to optical quality. The samples are glued onto a small graphite block to provide cooling during the irradiation process. Irradiations are carried out at the isochron cyclotron of the Helmholtz-Institut für Strahlen- und Kernphysik, Universität Bonn. We use ^{3}He ions with an energy of 40 MeV. The total current directed onto the crystal is about 40 nA, and each irradiation deposits a dose of 130 μC in the sample, corresponding to an exposure duration of 1 hour.

To create a channel waveguide, it is necessary to maintain a region inside the crystal which will not be exposed to the ion beam. To realize this, the geometry depicted in Fig. 1a is used. A thin tungsten blade is spanned in front of the crystal surface that is heading towards the ion beam. The tungsten blade has a thickness of 25 μm and a width of 1 mm (with respect to the direction of the ion current). It absorbs the ions and creates an ion beam shadow on the crystal where hence no irradiation takes place. Outside the shaded area the full current is loaded onto the crystal. The tungsten blade is mounted about 200 μm below the crystal edge; thus, the shadow of the irradiation is also 200 μm below the top surface. A second irradiation takes place with a similar geometry; but the crystal is turned by 90°.

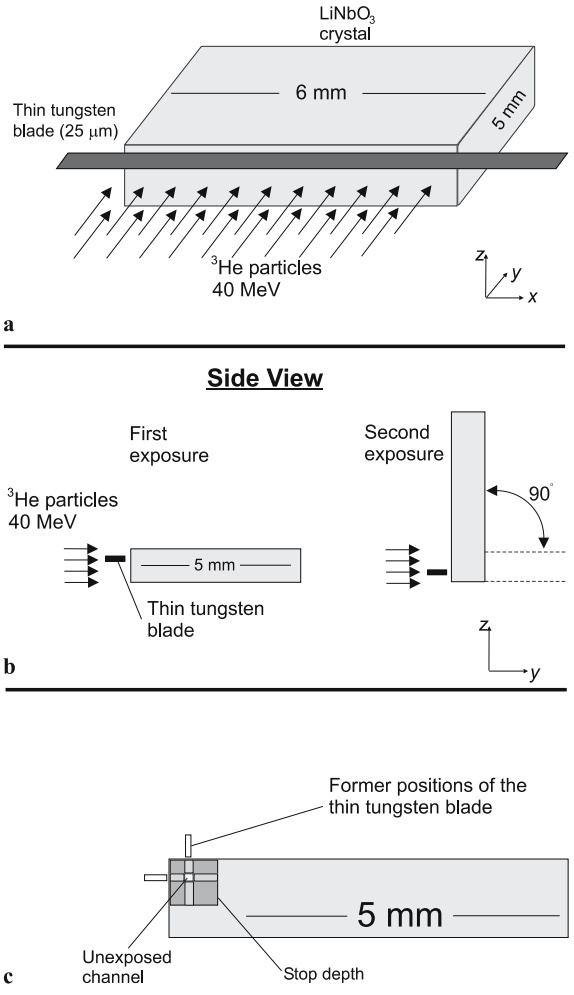

FIGURE 1 Geometries used for the exposure of $LiNbO_3$ crystals with ^3He. (**a**) A thin tungsten blade spanned in front of the crystal blocks the ions and creates a thin shadow yielding a non-exposed layer during one irradiation treatment. (**b**) The side view shows two exposure treatments carried out under an angle of 90°. After the first treatment, the crystal is rotated. (**c**) As a result of the exposures, two ion beam shadows beyond the former positions of the tungsten blade are formed. In the area where the two shadow layers cross, an unexposed channel is created

This is illustrated in Fig. 1b. Looking at the crystal from the side, a small channel in the crossing of the the two shadows is formed which is not irradiated by any of the two treatments (see Fig. 1c). Inside the shadows the material is irradiated only once. The stop depth of the ions (range about 0.6 mm) is indicated in Fig. 1c, too: It lies far away from the area of interest. In conclusion, one single treatment provides a non-irradiated layer, two crossed treatments yield a non-irradiated channel. We use this geometry, a kind of small scale tomography using only two angles, as a simple proof of principle.

After the irradiation the samples are optically investigated. Measurements are carried out with a typical fiber-to-waveguide coupling setup, as shown in Fig. 2. The light of a He-Ne laser ($\lambda = 632.8\,\text{nm}$) is coupled into a monomode fiber. The bare end of this fiber emits a divergent cone of non-polarized light. The crystal can be adjusted with respect to the fiber end. The light travels through the crystal and leaves it at the output surface; this surface is imaged onto a screen which is photographed by a CCD camera. Thus the spatial distribution of light passing through the output surface can be determined. The polarization of the light beyond the crystal can be selected by means of a dichroic polarizer.

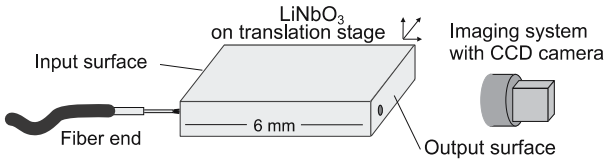

FIGURE 2 Fiber-to-waveguide setup. The crystal can be aligned with respect to the fiber end

3 Results

One sample in which the crystallographic c axis is oriented parallel to the non-irradiated channel is prepared. Figure 3 shows a picture of the (y, z)-surface of one side of an as-prepared crystal, taken through a microscope. In the photograph, the exposed area with a typical brownish color, which usually appears after our ion exposure [15], can be seen. Furthermore, the non-irradiated shadows of the two treatments and especially the crossing zone of these two shadows (where no brownish color is present) can be observed. The Bragg peak at the stop depth of the ions is also indicated.

The results of the optical wave propagation investigation are shown in Fig. 4. Part a shows the light distribution at the output surface when the light is coupled into the sample through the input surface at the position of the channel. A strong peak with large light intensity is observed. Figure 4b shows the light distribution when the light couples into the crystal far outside the irradiated area: A broad light cone is present. Please note that the grayscales of the two pictures, which correspond to the light intensity, are different: Part b is taken with a six times higher sensitivity; thus for the same grey level the intensity is six times lower compared to that in Fig. 4a.

Next, a second crystal irradiated in the same manner as described before, but with the c axis oriented perpendicular to the non-exposed channel, is also investigated. The light intensity at the output plane depends on the orientation of the dichroic polarizer. The results are presented in Fig. 5. Part a shows the light pattern for ordinarily polarized light. Again,

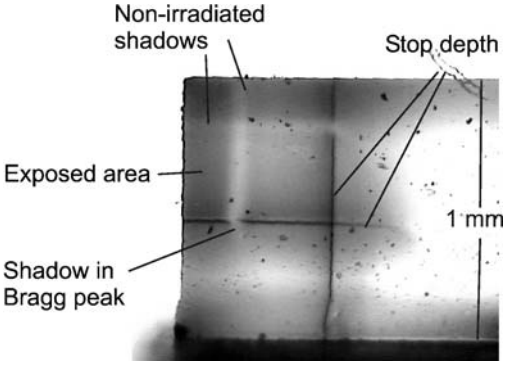

FIGURE 3 Photograph of an irradiated crystal. It shows the crystal edge, the irradiated areas with the two shadow layers which form a non-exposed channel, and the stop depth of the ions

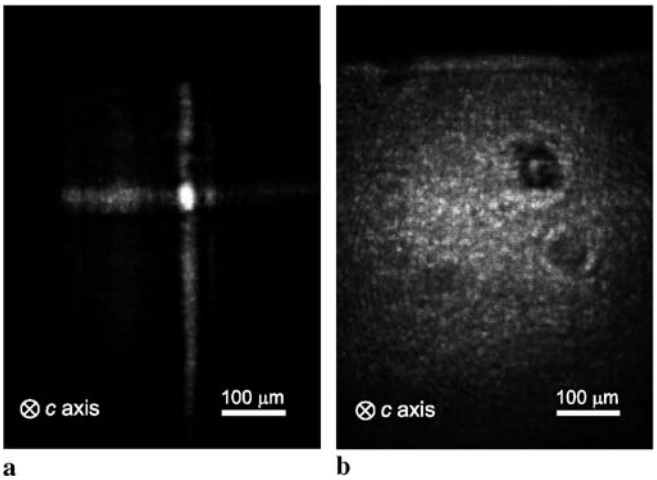

a b

FIGURE 4 Light distributions at the output surface of a sample with the *c* axis perpendicular to the surface plane (**a**) if the light is coupled into the non-exposed channel, and (**b**) if the light propagates through a non-irradiated area of the crystal. Part (**b**) is taken with a six times higher sensitivity compared to part (**a**)

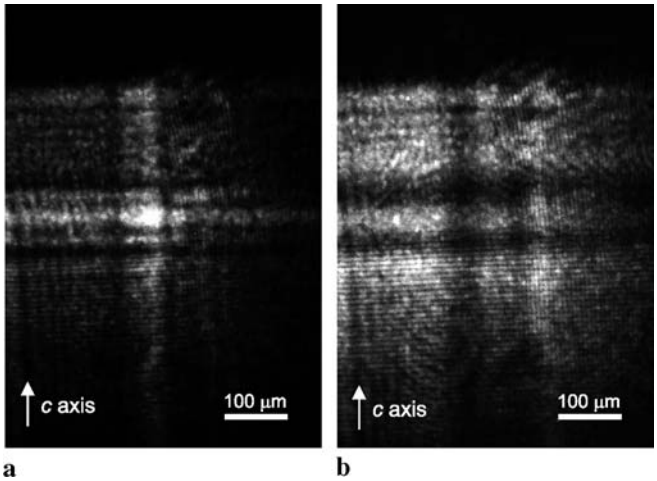

a b

FIGURE 5 Light distributions at the output surface of a sample where the *c* axis is parallel to the surface plane if (**a**) ordinary light polarization or (**b**) extraordinary light polarization is selected

a small bright area guiding the light is observed. Part b of Fig. 5, however, shows the result for extraordinarily polarized light. In the area of the non-irradiated channel, no light is guided.

4 Discussion

If light is fed into a reference region of the crystal that lies outside the treated area, it propagates divergently through the material and leaves the crystal through the output surface with a broad spatial distribution. In comparison, the light coupled into the non-irradiated channel within the treated area is obviously guided: it leaves the sample trough a tiny spot, and the intensity in this spot is much larger compared to that in the non-guided case. This is clearly shown in Fig. 4. The waveguide is a direct consequence of the non-uniform irradiation pattern. The intensity distribution does not show any multimode-interference structure, indicating the presence of a monomode waveguide. The size of the spot is about 30 μm which fits excellently to the size of the ion beam shadow, determined by the thickness of our tungsten blades. However, some light is not caught in the waveguiding channel, but in the planes left/right and up/down with respect to the channel, corresponding to the layers that have collected an ion dose just from one of the exposure processes. This may be improved by an optimization of the exposure time and current, which will enhance the refractive-index contrast or by optimizing the irradiation geometry using tomographic approaches in order to create a more homogeneous non-irradiated area.

As Fig. 5 demonstrates, ordinarily polarized light is guided whereas extraordinarily polarized light is deflected out of the non-exposed channel. This behavior proves that in the irradiated areas the refractive index n_o is reduced, which is in accordance with previously published data [15]. The index for extraordinarily polarized light Δn_e, however, is enlarged by the exposure treatment yielding a polarization-selective waveguide. Thus integrated-optical elements like a polarizer may be supplied by our technique.

From the data presented in Fig. 4, the fidelity of our waveguide can be estimated if one integrates the collected light over the small spot (Fig. 4a) or the broad cone (Fig. 4b), respectively. The ratio of these values yields a first estimate for the losses, because it relates the guided light intensity to the total light intensity sent into the crystal: We obtain a light intensity ratio of $0.5 = 3$ dB, which yields a loss per length of 5 dB/cm. The reason for these rather high losses may be imperfect waveguide preparation that results from scattering of ions due to imperfect edge preparation of our tungsten blade; straggling of the ions within the material is not significant due to the high particle energy.

Please note that light is guided in an unexposed section of the crystal; thus, once the edges of this waveguide are well prepared, superior low losses are expected. The evanescent sections of the waveguide modes may penetrate into the exposed volumes, but radiation-induced absorption in these areas can be removed completely by moderate annealing treatments while most of the refractive-index changes are kept [15]. The emphasis of this work is to give the proof of principle that our technique works, and that it may be an interesting way to create embedded guiding structures, a feature that other waveguide preparation techniques do not provide. Improving exposure parameters (such as exposure time and current) and optimization of the geometry used (e.g., rotating the crystal around an ion beam or employing focused ion beams) should enable the fabrication of low-loss waveguides because no surface-induced disturbances are present; the light is guided deeply inside the material. More complex structures such as curved waveguides are possible, depending on the irradiation geometry used. Furthermore, the technique may be extended to the fabrication of periodic photonic structures: 2D waveguide arrays already cause a lot of attention, but our method promises to realize 3D waveguide lattices that are even more promising [16, 17].

5 Conclusion

Irradiation of $LiNbO_3$ crystals with spatially modulated distributions of high-energy ions like 40 MeV ^{3}He yield

a refractive-index pattern. The feasibility to create embedded waveguides in $LiNbO_3$ is demonstrated. A polarization dependence of the refractive-index changes enables the fabrication of integrated, polarization sensitive optical elements.

ACKNOWLEDGEMENTS Technical support of the cyclotron team of the Helmholtz-Institut, Universität Bonn, is highly appreciated. Financial support of the DFG (grant FOR 557) and the Deutsche Telekom AG is gratefully acknowledged.

REFERENCES

1 V. Leyva, G.A. Rakuljic, B. O'Conner, Appl. Phys. Lett. **65**, 1079 (1994)
2 S. Breer, K. Buse, Appl. Phys. B **66**, 339 (1998)
3 S. Breer, H. Vogt, I. Nee, K. Buse, Electron. Lett. **34**, 2419 (1999)
4 D. Psaltis, F. Mok, Sci. Am. **273**(5), 52 (1995)
5 R.M. Shelby, J.A. Hoffnagle, G.W. Burr, C.M. Jefferson, M.-P. Bernal, H. Coufal, R.K. Grygier, H. Guenther, R.M. Macfarlane, G.T. Sincerbox, Opt. Lett. **22**, 1509 (1997)
6 C. Becker, A. Greiner, T. Oesselke, A. Pape, W. Sohler, H. Suche, Opt. Lett. **23**, 1194 (1998)
7 R.C. Alferness, R.V. Schmidt, E.H. Turner, Appl. Opt. **18**, 4012 (1979)
8 W.E. Martin, Appl. Phys. Lett. **26**, 562 (1975)
9 W.K. Burns, A.B. Lee, A.F. Milton, Appl. Phys. Lett. **29**, 790 (1976)
10 V. Ramaswamy, M.D. Divino, R.D. Standley, Appl. Phys. Lett. **32**, 644 (1978)
11 J.L. Jackel, C.E. Rice, J.J. Veselka, Appl. Phys. Lett. **41**, 607 (1982)
12 R.V. Schmidt, I.P. Kaminow, Appl. Phys. Lett. **25**, 458 (1974)
13 D. Kip, Appl. Phys. B **67**, 131 (1998)
14 G.L. Destefanis, P.D. Townsend, J.P. Galliard, Appl. Phys. Lett. **32**, 293 (1978)
15 B. Andreas, K. Peithmann, K. Buse, K. Maier, Appl. Phys. Lett. **84**, 3813 (2004)
16 D.N. Christodoulides, F. Lederer, Y. Silberberg, Nature **424**, 817 (2003)
17 J.D. Johannopoulos, P.R. Villeneuve, S.H. Fan, Nature **386**, 143 (1997)